Analysis of Coupled Bimolecular Reaction Kinetics and Diffusion by Two-Color Fluorescence Correlation Spectroscopy: Enhanced Resolution of Kinetics by Resonance Energy Transfer

Erik F. Y. Hom and A. S. Verkman

The Graduate Group in Biophysics, Departments of Medicine and Physiology, and Cardiovascular Research Institute, University of California, San Francisco, California 94143-0521 USA

ABSTRACT In two-color fluorescence correlation spectroscopy (TCFCS), the fluorescence intensities of two fluorescently-labeled species are cross-correlated over time and can be used to identify static and dynamic interactions. Generally, fluorophore labels are chosen that do not undergo Förster resonance energy transfer (FRET). Here, a general TCFCS theory is presented that accounts for the possibility of FRET between reactants in the reversible bimolecular reaction, $A + B \underset{k_b}{\overset{k_f}{\longleftrightarrow}} C$, where k_f and k_b are forward and reverse rate constants, respectively (dissociation constant $K_d = k_b/k_f$). Using this theory, we systematically investigated the influence on the correlation function of FRET, reaction rates, reactant concentrations, diffusion, and component visibility. For reactants of comparable size and an energy-transfer efficiency of ~90%, experimentally measurable cross-correlation functions should be sensitive to reaction kinetics for $K_d > 10^{-8}$ M and $k_f \geq \sim 10^7\ M^{-1}s^{-1}$. Measured auto-correlation functions corresponding to donor and acceptor labels are generally less sensitive to reaction kinetics, although for the acceptor, this sensitivity increases as the visibility of the donor increases relative to the acceptor. In the absence of FRET or a significant hydrodynamic difference between reactant species, there is little effect of reaction kinetics on the shape of auto- and cross-correlation functions. Our results suggest that a subset of biologically relevant association–dissociation kinetics can be measured by TCFCS and that FRET can be advantageous in enhancing these effects.

INTRODUCTION

In fluorescence correlation spectroscopy (FCS), the spontaneous fluorescence fluctuations arising from a small probe volume within a fluorescent sample are temporally correlated to obtain information about the molecular processes that cause these fluctuations (Magde et al., 1972; Elson and Magde, 1974; Magde et al., 1974; Thompson, 1991). The shape of the correlation function is dependent upon the dynamics of the fluorescent particles in the probe volume, whereas the amplitude of the auto-correlation function at zero time is inversely proportional to the average number of particles (Elson and Magde, 1974; Thompson, 1991; Maiti et al., 1997; Van Craenenbroeck and Engelborghs, 2000). Hydrodynamic properties, particle concentration, fluorescence photophysics, conformational kinetics, aggregation state, and binding thermodynamics have been measured using FCS (Widengren et al., 1995; Bonnet et al., 1998; Haupts et al., 1998; Pack et al., 1999; Schwille et al., 1999; Tjernberg et al., 1999; Wohland et al., 1999; Chen et al., 2000; Heikal et al., 2000; Lamb et al., 2000; Langowski and Tewes, 2000; Rippe, 2000). The kinetics of slow intermolecular reactions (Rauer et al., 1996; Schwille et al., 1997a; Kettling et al., 1998; Meyer-Almes et al., 1998; Schüler et al., 1999) and, to a lesser extent, the kinetics of fast reversible intermolecular reactions (Elson and Magde, 1974; Icenogle and Elson, 1983; Haupts et al., 1998; Lamb et al., 2000; Bismuto et al., 2001), have also been measured using FCS.

The rate constants of very fast reactions can be deduced directly from the time-dependent decay of the correlation function. For slow reactions, rate constants are typically estimated indirectly by measuring reactant:product ratios as a function of time following a sudden change in reactant concentration (or a reaction initiation event) under pseudo first-order conditions. This latter approach is unlikely to be useful, however, when the time scale for kinetic relaxation is comparable to that needed to make numerous FCS measurements of reasonable quality (each typically >30 s). Moreover, a macroscopic concentration perturbation is required, which goes counter to the conceptual motivations of FCS as a nonperturbative method.

For FCS to be useful in measuring reaction kinetics, a sufficient number of reaction turnover events must be observed before reaction components diffuse out of the probe volume. What constitutes a "sufficient number" is not clear. If the time scales for reaction and diffusion are very different, approximations have been made that either incorporate the influence of kinetics at early times when they are fast, or neglect the effects of kinetics on the correlation curve-shape when they are slow (Widengren and Rigler, 1998). The precise conditions under which these approximations are appropriate are likewise not clear. Consequently, there is little in the literature to document the usefulness of FCS for studying reactions with moderate time kinetics.

Submitted December 22, 2001, and accepted for publication March 20, 2002.

Address inquiries to Erik Hom, 1246 Health Science East Tower, Univ. of California, San Francisco, CA 94143-0521. Tel.: 415-476-8530; Fax: 415-665-3847; E-mail: erikhom@cgl.ucsf.edu.

0006-3495/02/07/533/14 $2.00

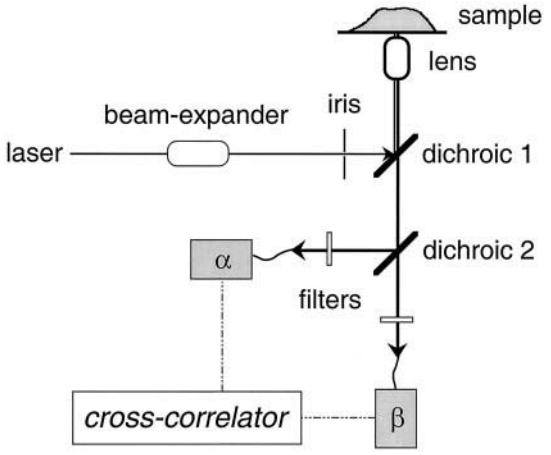

FIGURE 1 TCFCS measurement scheme. Schematic of a double-detector FCS apparatus in which emitted fluorescence is spectrally separated by a dichroic mirror and focused onto fiber-optic light guides coupled to detectors α and β.

In this paper, we assess the utility of FCS for studying bimolecular reaction kinetics. Based on the work of Schwille and co-workers (Schwille et al., 1997b; Kettling et al., 1998; Heinze et al., 2000), a general FCS theory is presented that applies to the experimental situation in which two detectors are used to monitor the fluorescence fluctuations arising from two fluorescently labeled, interacting species (Fig. 1). The influence of key parameters on experimentally detected auto- and cross-correlation curves are examined, including the reaction rate and reactant concentrations, and the diffusion and visibility of reaction components. Importantly, the two-color FCS (TCFCS) theory presented here includes the possibility of resonance energy transfer in the bound complex, which is shown to be of considerable value in enhancing the effects of reaction kinetics on experimentally measurable correlation functions.

THEORY

The double-detector correlation function

Consider an open system of particles containing m differently labeled fluorescent species. The goal is to extract information about the diffusion and reaction dynamics of these particles by temporally correlating the fluorescence fluctuations observed within a small probe volume, V. The experimentally accessible correlation function of the fluorescence fluctuations measured using two detector channels, x and y, can be defined as

$$G_{xy}(\tau) = \overline{\delta F^x(t) \cdot \delta F^y(t+\tau)}/(\overline{F^x} \cdot \overline{F^y}), \qquad (1)$$

where τ is the correlation time (the overline denotes a time average over a time $T \gg \tau$), $F^x(t)$ is the total fluorescence signal registered in channel x at a time t, and the fluorescence fluctuation about the mean is $\delta F^x(t) = \overline{F^x} - F^x(t)$. $G_{xy}(\tau)$ is the double-detector correlation function. The total fluorescence signal can be written as $F^x(t) = f^x(t) + b^x(t)$, where $f^x(t)$ is the fluorescence signal arising from all m fluorescent species at time t ($f^x(t) = \Sigma_i^m f_i^x(t)$) and $b^x(t)$ accounts for any uncorrelated background signal. It follows that,

$$G_{xy}(\tau) = \underbrace{\frac{(1 + \overline{b^x}/\overline{f^x})^{-1} \cdot (1 + \overline{b^y}/\overline{f^y})^{-1}}{\aleph_x \cdot \aleph_y}}_{} \times \underbrace{\left[\overline{\left(\sum_i^m \delta f_i^x(t)\right) \cdot \left(\sum_j^m \delta f_j^y(t+\tau)\right)} \Big/ (\overline{f_i^x} \cdot \overline{f_j^y})\right]}_{g_{xy}(\tau)}, \qquad (2)$$

where $g_{xy}(\tau)$ is the fluctuation correlation function for the m-particle system of interest, and $\aleph_x$ and $\aleph_y$ are correction factors (≤ 1) for the uncorrelated background. In practice, an offset term is sometimes added to Eq. 2 to account for any accidental correlation due to sample contamination or systematic error (Schwille et al., 1999; Wohland et al., 2001); we will assume this offset is negligible.

The time-dependent fluorescence fluctuation for the ith species monitored by detector channel x can be expressed as

$$\delta f_i^x(t) = \eta_i^x(\lambda_i) \int W(r) \cdot \delta C_i(\mathbf{r}, t)\, d\mathbf{r},$$

$$\eta_i^x(\lambda_i) = W_0 \cdot \varepsilon_i(\lambda_i) \cdot Q_i \cdot g_x, \qquad (3)$$

where $\delta C_i(\mathbf{r}, t)$ is the time-dependent fluctuation in the molar concentration of species i at spatial position $\mathbf{r}$, and $W(\mathbf{r})$ is a dimensionless function characterizing the illumination profile of the effective volume element normalized by W_0, the excitation amplitude of the illumination beam at the center of focus ($W(0) = 1$) (Mertz, 1998). λ_f is the wavelength of the illumination beam used to excite species i; ε_i and Q_i are the intensity-dependent absorptivity and fluorescence quantum yield; and g_x is the collection efficiency of detector channel x. $\eta_i^x(\lambda_i)$ is the x-detector visibility (or "molecular brightness") defined as the number of photons detected in channel x per second per molecule of i (Chen et al., 1999; Müller et al., 2000). The λ_i-dependence of η_i^x will hereafter be implicit.

$G_{xy}(\tau)$ can then be expressed in terms of diffusion/reaction kinetic parameters using Eq. 3 and by solving for δC_i according to the set of coupled reaction–diffusion equations at equilibrium,

$$\partial \boldsymbol{\delta C}(\mathbf{r}, \tau)/\partial \tau = (\mathbf{D} \cdot \nabla^2 + \mathbf{R}) \cdot \boldsymbol{\delta C}(\mathbf{r}, \tau),$$

where $\boldsymbol{\delta C}$ is the vector of concentration fluctuations for the m species, $\mathbf{D}$ is the vector of diffusion constants (assuming

no hydrodynamic coupling between components), and **R** is the linearized matrix of rate constants and equilibrium concentrations ($\bar{C}_i$) that describe the reaction mechanism (Elson and Magde, 1974; Bernasconi, 1976; Thompson, 1991). By spatial Fourier transform,

$$\frac{\partial \delta\tilde{\mathbf{C}}(\mathbf{q}, \tau)}{\partial \tau} = \mathbf{M} \cdot \delta\tilde{\mathbf{C}}(\mathbf{q}, \tau), \tag{4}$$

where $\mathbf{M} \equiv (\mathbf{R} - \mathbf{D} \cdot \mathbf{q}^2 \cdot \mathbf{I})$ and **I** is the identity matrix, which can be solved by standard matrix methods (Elson and Magde, 1974; see Appendix A).

Using solutions to Eq. 4, $G_{xy}(\tau)$ can be written as an integral over Fourier spatial frequencies (**q**) and ultimately expressed as

$$G_{xy}(\tau) = \aleph_x \aleph_y \cdot \sum_i^m \sum_j^m d_{ij}^{xy} \cdot h_{ij}(\tau), \tag{5}$$

where d_{ij}^{xy} is the detectability weight, and $h_{ij}(\tau)$ is the component correlation function for species *i* and *j*. d_{ij}^{xy} can be expressed as

$$d_{ij}^{xy} = \frac{\bar{N}_\Sigma^{-1} \cdot [r_i^x \, r_j^y \sqrt{\chi_i \chi_j}]}{\left(\sum_i^m r_i^x \, \chi_i\right)\left(\sum_j^m r_j^y \, \chi_j\right)}, \tag{6}$$

where $\bar{N}_\Sigma$ is the average total number of particles in the observation volume, χ_i is the mole fraction of the *i*th species, and r_i^x is the *x*-detector visibility of species *i* normalized by the *x*-visibility of the brightest singly labeled species. The component correlation function, $h_{ij}(\tau)$, is defined as

$$h_{ij}(\tau) = h_{ji}(\tau) = \int Z_{ij}(\mathbf{q}, \tau) \cdot \Omega(\mathbf{q}) \, d\mathbf{q}, \tag{7}$$

where the function $Z_{ij}(\mathbf{q}, \tau)$ characterizes how spontaneous particle number fluctuations are spatio-temporally dissipated (see Appendix A) and $\Omega(\mathbf{q})$ is a geometric weighting factor that is dependent upon characteristics of the observation volume having units of reciprocal volume. For an *n*-photon-excited three-dimensional Gaussian-ellipsoidal (3DG) volume, $V = (\pi/n)^{3/2} w_r^2 w_z$ and

$$\Omega(\mathbf{q}) = \left(\frac{w_r^2 w_z}{(4n\pi)^{3/2}}\right) \exp[-w_r^2(q_x^2 + q_y^2)/4n] \times \exp[-w_z^2 \, q_z^2/4n],$$

where w_r and w_z are the radial and axial waists of the volume element, respectively. In general, Eq. 7 cannot be integrated analytically and component correlation functions, $h_{ij}(\tau)$, must be determined by numerical integration.

It is assumed that the particles under study are chemically ideal. Practically, this means that, if the particles interact, they do so without any memory effects at a time $\tau = 0_+$ such that $\tau_{TS} \ll 0_+ \ll \tau_{reac}$, τ_{TS} being the average lifetime of the reaction transition state that separates experimentally distinguishable chemical species, and τ_{reac}, the average lifetime of the particles before they react (Chandler, 1987). With this assumption, $h_{ij}(0_+) = \delta_{ij}$ (Elson and Magde, 1974), and only the component auto-correlation functions contribute to the initial detector correlation amplitude, $G_{xy}(0_+)$. As needed below, it is convenient to write the detector correlation function as a product of this amplitude and a shape function, $H_{xy}(\tau)$,

$$G_{xy}(\tau) = G_{xy}(0_+) \cdot H_{xy}(\tau), \tag{8}$$

where $H_{xy}(0_+) = 1$ and $H_{xy}(\infty) = 0$.

Application to reversible bimolecular reactions

The above formalism is applicable to an arbitrary *m*-particle system. Our analysis will focus exclusively on reversible bimolecular reactions of the form,

$$A + B \underset{k_b}{\overset{k_f}{\leftrightarrow}} C,$$

where k_f and k_b are the forward and backward rate constants, respectively, and $K_d = k_b/k_f$ is the equilibrium dissociation constant. We assume that reactant species A and B are labeled with fluorophores that are distinct in their emission spectra upon exciting at wavelengths λ_A and λ_B, and monitored by detector channels α and β, respectively (Fig. 1). Using Eqs. 5 and 6, the double-detector correlation functions, $G_{xy}(\tau)$, can be expressed as a linear combination of component correlation functions, $h_{ij}(\tau)$. Assuming there is zero bleed-through fluorescence registered in detector channels ($r_A^\beta = r_B^\alpha = 0$) (see Appendix B), the two detector auto-correlation functions are

$$G_{\alpha\alpha}(\tau) = (\aleph_\alpha^2/\bar{N}_A)\,(\theta_A^2/(\theta_A^2 + r_C^\alpha \theta_C^2)^2) \times [\theta_A^2 h_{AA}(\tau) + (r_C^\alpha)^2\,\theta_C^2 h_{CC}(\tau) - 2 r_C^\alpha \theta_A \theta_C h_{AC}(\tau)], \tag{9}$$

$$G_{\beta\beta}(\tau) = (\aleph_\beta^2/\bar{N}_B)\,(\theta_B^2/(\theta_B^2 + r_C^\beta \theta_C^2)^2) \times [\theta_B^2 h_{BB}(\tau) + (r_C^\beta)^2\,\theta_C^2 h_{CC}(\tau) - 2 r_C^\beta \theta_B \theta_C h_{BC}(\tau)],$$

and the double-detector cross-correlation function is

$$G_{\alpha\beta}(\tau) = (\aleph_\alpha \aleph_\beta/\bar{N}_C)\,(\theta_C^2/((\theta_A^2 + r_C^\alpha \theta_C^2)\,(\theta_B^2 + r_C^\beta \theta_C^2))) \times [r_C^\alpha r_C^\beta \theta_C^2 h_{CC}(\tau) + \theta_A \theta_B h_{AB}(\tau) - r_C^\beta \theta_A \theta_C h_{AC}(\tau) - r_C^\alpha \theta_B \theta_C h_{BC}(\tau)], \tag{10}$$

where $\theta_A = \sqrt{\chi_A/\chi_C}$, $\theta_B = \sqrt{\chi_B/\chi_C}$, and $\theta_C = -1$. The correlation functions in Eqs. 9 and 10 may be expressed explicitly in terms of the dissociation constant, K_d, and the

total reactant concentrations, $\bar{C}_A^{tot}$ and $\bar{C}_B^{tot}$, using the relations,

$$\theta_A^2 = \frac{\bar{C}_A^{tot}}{\bar{C}_C} - 1 \qquad \text{and} \qquad \theta_B^2 = \frac{\bar{C}_B^{tot}}{\bar{C}_C} - 1$$

with

$$\bar{C}_C = [(\bar{C}_A^{tot} + \bar{C}_B^{tot} + K_d) - \sqrt{(\bar{C}_A^{tot} + \bar{C}_B^{tot} + K_d)^2 - 4\bar{C}_A^{tot}\bar{C}_B^{tot}}]/2. \quad (11)$$

Förster resonance energy transfer

If species A and B are labeled with donor and acceptor fluorophores, respectively, which undergo Förster resonance energy transfer (FRET) with mean efficiency E upon forming complex C, then the relative α- and β-visibilities for C can be written as

$$r_C^\alpha = (1 - E) \qquad \text{and} \qquad r_C^\beta = (1 + [\eta_A^\alpha/\eta_B^\beta]E). \quad (12)$$

For simplicity, we have assumed an ideal case in which there is no detector bleed-through (see Appendix B).

The correlation function amplitude: $G_{xy}(0_+)$

As given by Eq. 8, the detector correlation function can be expressed as a product of the amplitude at $\tau = 0_+$ and a unimodal shape factor. With perfect fluorophore discrimination ($r_B^\alpha = r_A^\beta = 0$), the correlation function amplitudes can be written as

$$\begin{aligned} G_{\alpha\alpha}(0_+) &= (\aleph_\alpha^2/\bar{N}_A)\theta_A^2[\theta_A^2 + (r_C^\alpha)^2]/[\theta_A^2 + r_C^\alpha)^2], \\ G_{\beta\beta}(0_+) &= (\aleph_\beta^2/\bar{N}_B)\theta_B^2[\theta_B^2 + (r_C^\beta)^2]/[\theta_B^2 + r_C^\beta)^2], \\ G_{\alpha\beta}(0_+) &= (\aleph_\alpha\aleph_\beta/\bar{N}_C)\,[r_C^\alpha r_C^\beta]/[(\theta_A^2 + r_C^\alpha)(\theta_B^2 + r_C^\beta)]. \end{aligned} \quad (13)$$

Here, it is assumed that the fluorescence energy transfer event is much faster than the time $\tau = 0_+$ ($\tau_{FRET} \ll 0_+ \ll \tau_{reac}$). Using Eq. 13, the average number of reactant and complex molecules in the observation volume, $\bar{N}_A$, $\bar{N}_B$, and $\bar{N}_C$, can be solved for simultaneously and explicitly. Although these expressions are quite lengthy for the case at hand (see Appendix C), they simplify if no spectral changes occur upon complex formation (i.e., $r_C^\alpha = r_C^\beta = 1$) (Schwille et al., 1997b; Kettling et al., 1998; Heinze et al., 2000):

$$\begin{aligned} \bar{N}_C &= \aleph_\alpha\aleph_\beta \cdot \frac{G_{\alpha\beta}(0_+)}{G_{\alpha\alpha}(0_+)\cdot G_{\beta\beta}(0_+)}, \\ \bar{N}_A &= \frac{\aleph_\alpha^2}{G_{\alpha\alpha}(0_+)} - \bar{N}_C, \\ \bar{N}_B &= \frac{\aleph_\beta^2}{G_{\beta\beta}(0_+)} - \bar{N}_C. \end{aligned} \quad (14)$$

Diffusion and reaction time scales

To assess whether reaction kinetics influence the shape of double-detector correlation functions in an experimentally detectable manner, it is helpful to define characteristic diffusion and reaction times, $\tau_{diff} \equiv w_r^2/4n_P\langle D\rangle$ and $\tau_{reac} \equiv (k_f[\bar{C}_A + \bar{C}_B] + k_b)^{-1}$. Here, $\langle D\rangle$ is the ensemble-averaged diffusion coefficient of the particles in volume V (Rigler et al., 1992), and n_P is the number of photons used to excite a Gaussian-cylindrical or -ellipsoidal probe volume of radial waist, w_r (for a 2-photon excited Gaussian–Lorentzian volume, $n_P = 1.5$ (Mertz, 1998)). The difference in diffusion and reaction time scales can then be expressed using the dimensionless metric, ζ,

$$\zeta \equiv \frac{\tau_{diff}}{\tau_{reac}} = \left(\frac{w_r^2}{4n_P\langle D\rangle}\right)\cdot\frac{k_b}{\Gamma}, \quad (15)$$

where $\Gamma = (1/\theta_A^2 + 1/\theta_B^2 + 1/\theta_C^2)^{-1}$. ζ characterizes the number of reaction turnover events observed per dwell time for the ensemble of particles within the probe volume; within this time, about half of the particles diffusively exchange with those outside the volume (Mertz, 1998). The parameter Γ characterizes the position of reaction equilibrium. Using Eq. 11, Γ may be expressed explicitly in terms of the dissociation constant, K_d, and the total reactant concentrations, $\bar{C}_A^{tot}$ and $\bar{C}_B^{tot}$,

$$\Gamma = K_d/\sqrt{(\bar{C}_A^{tot} + \bar{C}_B^{tot} + K_d)^2 - 4\bar{C}_A^{tot}\bar{C}_B^{tot}}. \quad (16)$$

When $K_d < (\bar{C}_A^{tot} = \bar{C}_B^{tot})$ (complex formation is favored), $\Gamma \to 0$; when $K_d = (\bar{C}_A^{tot} = \bar{C}_B^{tot})$, $\Gamma = \sqrt{1/5}$; when $K_d > (\bar{C}_A^{tot} = \bar{C}_B^{tot})$ (reactants are favored), $\Gamma \to 1$.

METHODS

Simulations of detector correlation functions, $G_{xy}(\tau)$, were performed using Mathematica 4.1 (Wolfram Research Inc., Champaign, IL) on a 1.2-GHz Athlon processor, 256-MB Gateway computer (Linux OS). Eigenvalues and eigenvectors of the matrix M_{sym} were solved and $Z_{ij}(\mathbf{q}, \tau)$ expressions constructed symbolically as described in Appendix A. An $\Omega(\mathbf{q})$ function corresponding to either a one- or two-photon-excited Gaussian-ellipsoid volume was used. When required, correlation functions were integrated by numerical cubature to six-digits of precision using an adaptive Genz–Malik algorithm. Integrations were performed in reciprocal $\mathbf{q}$-space over a range corresponding to $x_{min} \le |x| \le \infty$ with $x_{min} = w_r/10$ in a single dimension; identical results were obtained to within six-digit precision with a discretization of $x_{min} = w_r/1000$. The correlation function integration protocol was verified by comparison with correlation function curves generated using analytical expressions for the case in which $D_A = D_B = D_C$ and those derived by Elson and Magde (1974) in the limit of $D_A = D_C \ll D_B$.

To assess whether detector correlation shape functions for a system with coupled reaction–diffusion, $H_{xy}^{reac\text{-}diff}(\tau)$, are experimentally distinguishable from those expected from a comparable system without reaction, $H_{xy}^{diff}(\tau)$, the variance between sets of curves were compared using the F-statistic, $F_{xy} = \langle\chi^2_{\nu_{diff}}/\chi^2_{\nu}\rangle_{N_{exp}}$ (Bevington and Robinson, 1992), where the brackets denote an average over N_{exp} correlation curves. χ^2_ν and $\chi^2_{\nu_{diff}}$ are the reduced

chi-squares that characterize the difference between the data, $H_{xy}(\tau_i)$, and the best-fit reaction–diffusion model or diffusion-only model, respectively:

$$\chi^2_\nu = \frac{1}{\nu}\sum_i^{N_d}\left(\frac{H_{xy}^{\text{reac-diff}}(\tau_i) - H_{xy}(\tau_i)}{\sigma_{xy}(\tau_i)}\right)^2,$$

and (17)

$$\chi^2_{\nu_{\text{diff}}} = \frac{1}{\nu_{\text{diff}}}\sum_i^{N_d}\left(\frac{H_{xy}^{\text{diff}}(\tau_i) - H_{xy}(\tau_i)}{\sigma_{xy}(\tau_i)}\right)^2,$$

where ν and ν_{diff} are the number of degrees of freedom for the fit (number of data points minus number of fitting parameters), $\sigma(\tau_i)$ is the standard deviation for the $H_{xy}(\tau_i)$ data, and N_d is the total number of time points used. Expressing $H_{xy}(\tau_i)$ as $\bar{H}_{xy}(\tau_i) + \{\phi_i\}$, with $\bar{H}_{xy}(\tau_i)$ corresponding to a reaction–diffusion parent function and $\{\phi_i\}$, a random number sampled from a Gaussian distribution of mean zero and variance $\sigma^2(\tau_i)$,

$$F_{xy} = \left\langle \left(\frac{\nu}{\nu_{\text{diff}}}\right)\left(\frac{\sum_i^{N_d}([H_{xy}^{\text{diff}}(\tau_i) - \bar{H}_{xy}(\tau_i)] + \{\phi_i\})^2}{\sum_i^{N_d}([H_{xy}^{\text{reac-diff}}(\tau_i) - \bar{H}_{xy}(\tau_i)] + \{\phi_i\})^2}\right)\right\rangle_{N_{\text{exp}}}. \quad (18)$$

F-statistics were computed using $N_{\text{exp}} = 50$, assuming the difference between best-fit values, $H_{xy}^{\text{reac-diff}}(\tau_i)$, and the parent function used to generate the simulated data, $\bar{H}_{xy}(\tau_i)$, is negligible relative to $\{\phi_i\}$. $\sigma^2(\tau_i)$ values were estimated using an analytical formula derived by Koppel (1974), validated by Meseth et al. (1999) and Wohland et al. (2001), and modified for the case in which data is acquired via two detectors and normalized by $G_{xy}(0_+)$ (see Note 1):

$$\sigma^2(\tau_i) = \left(\frac{\Delta t}{T}\right) \times \left(\frac{[1 + H_{xy}^2(\Delta t)]\,[1 + H_{xy}^2(\tau_i)]}{[1 - H_{xy}^2(\Delta t)]} + 2H_{xy}^2(\tau_i)\left(\frac{\tau_i}{\Delta t}\right) + \frac{2[1 + H_{xy}^2(\tau_i)]}{\sqrt{\langle n_x\rangle\langle n_y\rangle}\,G_{xy}(0_+)} + \frac{[1 + G_{xy}(0_+)H_{xy}(\tau_i)]}{\langle n_x\rangle\langle n_y\rangle\,G_{xy}^2(0_+)}\right). \quad (19)$$

Δt is the detection-channel sampling width; in practice, fluorescence intensities are monitored over a series of time bins of varying duration and correlated as photon counts per bin (Geerts, 1983; Schatzel et al., 1988; Thompson, 1991; Wohland et al., 2001). $\langle n_x\rangle$ is the average number of photon counts registered in detector channel x in a given Δt, $\langle n_x\rangle = (\sum_i \eta_i^x \bar{N}_i + b^x)\cdot\Delta t$. A value of $\Delta t = \tau/10$ and 25 τ_i-divisions per log τ were used in the calculation of F_{xy} (Eq. 18), which approximates the quasi-logarithmic binning structure of available hardware correlator cards (Meseth, 1996; Wohland et al., 2001. Eq. 19 typically overestimates the true variance of the data, particularly at long τ values, but is qualitatively correct (Rigler et al., 1993; Meseth et al., 1999; Wohland et al., 2001); Eq. 19 becomes more accurate as the number of particles in the probe volume contributing to the mean fluorescence increases (Koppel, 1974; Qian, 1990; Kask et al., 1997). F_{xy} were calculated using a τ-range of $\min[\tau_{\text{reac}}, \tau_{\text{diff}}]\cdot 10^{-2}$ to $\max[\tau_{\text{reac}}, \tau_{\text{diff}}]\cdot 10^2$, amounting to $N_d \sim$ 100–200 data points. $\tau = 0_+$ was set equivalent to $\min[\tau_{\text{reac}}, \tau_{\text{diff}}]\cdot 10^{-3}$. A minimum τ-range of four orders of magnitude (when $\tau_{\text{reac}} \sim \tau_{\text{diff}}$) is a conservative estimate of what is used experimentally to fit correlation data.

Given the number of degrees of freedom (ν and ν_{diff}) and a value for F_{xy}, a reaction–diffusion model can be considered a better descriptor of the simulated correlation data than a diffusion-only model to within a confidence level dictated by the F-distribution (Bevington and Robinson, 1992). For calculations with $N_d \sim \nu \sim \nu_{\text{diff}} \sim$ 100–200, an F_{xy} value of 1.3 implies that a reaction–diffusion model can be considered a better descriptor of the data with a p-value of 0.09–0.002. The validity of our F_{xy} calculation approach was confirmed by reproducing F-statistic values of Meseth et al. (1999) for conditions in which the auto-correlation function curves between a one-component diffusing system and a two-component diffusing system could be distinguished with a p-value of 0.01.

RESULTS

Basic features of $G_{xy}(\tau)$

The experimentally measured detector correlation functions are linear combinations of component correlation functions, $h_{ij}(\tau)$, weighted by detectablity factors, d_{ij}^{xy}, for each fluorescent species in the sample (Eq. 5). These detectability factors are a function of both the mole fraction, χ_i, and the relative visibility properties, r_i^x, for each species (Eq. 6). By using spectrally distinct reactant labels and monitoring fluorescence using two detectors, additional information is available to determine the kinetics of the reaction,

$$A + B \underset{k_b}{\overset{k_f}{\leftrightarrow}} C.$$

In Fig. 2, the detector correlation functions for such a reaction (in the absence of energy transfer, $E = 0$), are shown schematically as a sum of component correlation functions. The total reactant concentrations and dissociation constant for the reaction were set to $\bar{C}_A^{\text{tot}} = \bar{C}_B^{\text{tot}} = K_d = 10^{-8}$ M with both reactants equally visible to their intended detector ($\eta_A^\alpha = \eta_B^\beta$). The number of reaction turnover events per diffusive dwell time, ζ (Eq. 15), was set to 100 with equal diffusion coefficients for A, B, and C. Each of the component auto-correlation functions, $d_{ii}^{xy}\cdot h_{jj}(\tau)$, decays monotonically with two shoulders, the first occurring at $\tau = \tau_{\text{reac}}$ and the second at $\tau_{\text{diff}} = \zeta\cdot\tau_{\text{reac}}$. For this case in which $\bar{C}_A^{\text{tot}} = \bar{C}_B^{\text{tot}} = K_d$, $\chi_C = 0.62\cdot(\chi_A = \chi_B)$, so that component auto-correlation contributions of C are smaller than those of A or B,

$$d_{CC}^{xy}\cdot h_{CC}(0_+) < (d_{AA}^{xy}\cdot h_{AA}(0_+) \sim d_{BB}^{xy}\cdot h_{BB}(0_+)).$$

In contrast, the component cross-correlation functions start from zero, increase over a characteristic time $\tau \sim \tau_{\text{reac}}$, and decrease due to diffusional decorrelation at a later time $\tau \sim \tau_{\text{diff}}$. By mass action, a small, spontaneous increase in the concentration of A or B would lead to a comparable increase in the formation of complex C at a later time τ_{reac}; thus, reactants are positively cross-correlated with C ($h_{AC}(\tau) > 0$ and $h_{BC}(\tau) > 0$). Similarly, a small, spontaneous increase in the concentration of one reactants would

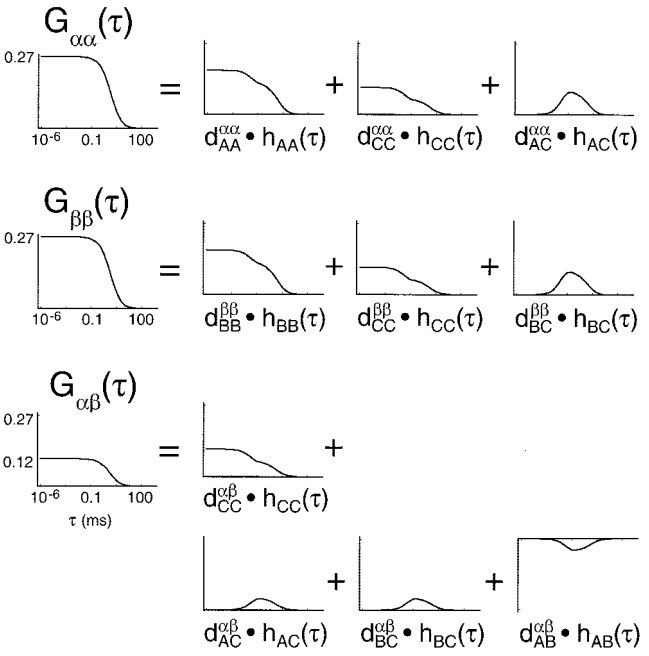

FIGURE 2 Detector correlation functions are a linear combination of component contributions. Double-detector auto- and cross-correlation functions ($G_{\alpha\alpha}(\tau)$, $G_{\beta\beta}(\tau)$, and $G_{ab}(\tau)$) for the reversible bimolecular reaction, A + B $\leftrightarrow^{k_f}_{k_b}$ C, shown as a sum of component correlation functions, $h_{ij}(\tau)$, weighted by detectability factors, d^{xy}_{ij} (Eq. 6). Detector channels α and β monitor the fluorescence from species A and B, respectively. Parameters (assuming two-photon excited 3D-Gaussian-ellipsoidal volume): $w_r = 0.48$ μm, $\kappa = 2.8$, $\bar{C}^{tot}_A = \bar{C}^{tot}_B = K_d = 10^{-8}$ *M*, $D_A = D_B = D_C = 8.5 \times 10^{-7}$ cm^2/s, $\eta^\alpha_A = \eta^\beta_B = 15$ kHz, and $\zeta = 100$.

lead to a decrease in the concentration of the other reactant so that reactants are negatively cross-correlated ($h_{AB}(\tau) < 0$). For the case shown,

$$d^{\alpha\beta}_{AC} \cdot h_{AC}(\tau) = d^{\alpha\beta}_{BC} \cdot h_{BC}(\tau) = -d^{\alpha\beta}_{AB} \cdot h_{AB}(\tau).$$

In the absence of hydrodynamic differences and energy transfer between particles, the component auto-correlation and cross-correlation contributions sum to yield detector correlation functions, $G_{xy}(\tau)$, with a single, smooth shoulder. As given by Eq. 8, it is useful to express $G_{xy}(\tau)$ as the product of a shape function, $H_{xy}(\tau)$, and an amplitude factor, $G_{xy}(0_+)$. Below, we examine the influence of FRET, reaction kinetics, and differential visibilities of the reactants on $H_{xy}(\tau)$ and $G_{xy}(0_+)$, with the goal of determining conditions under which reaction would influence $G_{xy}(\tau)$ to permit experimental determination of kinetic parameters.

Determining bimolecular reaction kinetics by analysis of $H_{xy}(\tau)$

In principle, kinetic parameters can be deduced from an analysis of the measured correlation decay. By toggling between different observable reaction states—states that may be characterized by different intrinsic hydrodynamic and fluorescence properties—kinetic interconversion indirectly modifies the shape of the detector correlation function. We consider first and mainly the "worse-case" scenario in which $D_A = D_B = D_C$, so that reaction components can only be resolved based on differences in their fluorescence characteristics. In this case, analytical forms for $H_{xy}(\tau)$ exist in which the effects of reaction and diffusion can be decoupled (see Appendix A; Elson and Magde, 1974; Thompson, 1991). For a 3DG volume,

$$H_{xy}(\tau) = \left(1 + \frac{\tau}{\tau_{diff}}\right)^{-1}\left(1 + \frac{\tau}{\kappa^2\tau_{diff}}\right)^{-1/2} \times \sum_i^m \sum_j^m d^{xy}_{ij}\left[\delta_{ij} + \frac{\Gamma}{\theta_i\theta_j}(e^{-\tau/\tau_{reac}} - 1)\right] \Bigg/ \sum_i^m \sum_j^m d^{xy}_{ij}, \quad (20)$$

where κ (termed the structure factor) is the axial:radial ratio of the observation volume, w_z/w_r (Langowski and Tewes, 2000). The term before the double sum of Eq. 20 accounts for correlations arising from diffusion alone whereas the bracketed term accounts for correlations due to reaction.

Energy transfer enhances the influence of reaction kinetics on $H_{xy}(\tau)$

Example detector auto- and cross-correlation shape functions, $H_{xy}(\tau)$ (Eq. 20), are shown in Fig. 3 for different E in the presence of reaction. A typical two-photon 3DG volume of radial waist $w_r = 0.48$ μm and $\kappa = 2.8$ (Heinze et al., 2000) was used, with an average of one reaction event observed per diffusive dwell time (i.e., $\zeta = 1$: $\tau_{reac} = \tau_{diff}$), $\eta^\alpha_A = \eta^\beta_B = 15$ kHz, and $K_d = 10^{-6}$ M, $\bar{C}^{tot}_A = \bar{C}^{tot}_B = 10^{-8}$ M. For the detector auto-correlation functions, as E increases, the presence of reaction kinetics causes the curves to shift to smaller τ. For the case shown, however, the reaction kinetic effects are very small. As E increases, reaction significantly changes the shape of the detector cross-correlation function: contributions from the component cross-correlation functions, $d^{\alpha\beta}_{AC} \cdot h_{AC}(\tau)$ and $d^{\alpha\beta}_{BC} \cdot h_{BC}(\tau)$, increase dramatically (not shown), causing the shoulder in $H_{\alpha\beta}(\tau)$ to shift upwards to values greater than 1 (see Note 2).

The FRET-enhanced effects of reaction kinetics on $H_{xy}(\tau)$ can be augmented by an increase in ζ

ζ characterizes the number of reaction turnover events observed per diffusive dwell time for the particles in the probe volume, V (Eq. 15). Figure 4 *A* shows the effects of ζ, in conjunction with E, on the detector cross-correlation shape function. Using similar parameters as in Fig. 3, a ten-fold increase in ζ ($\tau_{reac} < \tau_{diff}$) remarkably enhances the effects of kinetics on the cross-correlation function curve shape in synergy with E. A ten-fold decrease in ζ significantly diminishes these E-induced enhancements. Similar trends

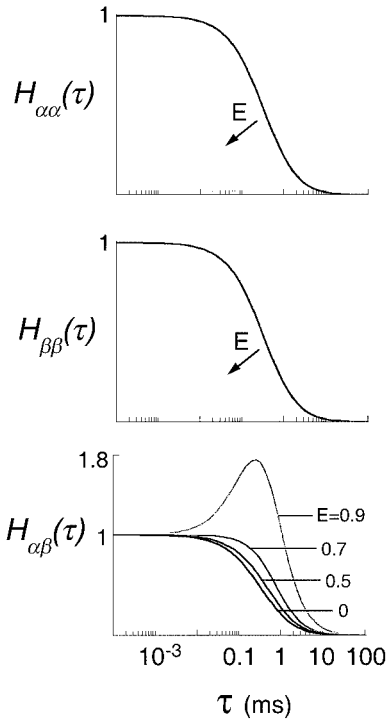

FIGURE 3 Energy transfer enhances the influence of chemical reaction on the shape of the detector correlation functions. Detector correlation shape functions, $H_{xy}(\tau)$ (Eq. 8), plotted as a function of E. Arrows point in the direction of increasing energy transfer between donor reactant A and acceptor reactant B, with $E = 0$, 0.5, 0.7, and 0.9. An average of one reaction turnover for every diffusive passage through the probe volume ($\zeta = 1$) was assumed. Parameters: $w_r = 0.48$ μm, $\kappa = 2.8$, $\bar{C}_A^{tot} = \bar{C}_B^{tot} = 10^{-8}$ M, $K_d = 10^{-6}$ M, $D_A = D_B = D_C = 8.5 \times 10^{-7}$ cm^2/s, and $\eta_A^\alpha = \eta_B^\beta = 15$ kHz.

were observed for the detector auto-correlation functions, although the effects are less obvious (not shown). Importantly, if $D_A = D_B = D_C$ and $E = 0$, the presence of reaction cannot be detected no matter how many reaction events are observed per dwell time.

The FRET-enhanced effects of reaction kinetics on $H_{xy}(\tau)$ can be augmented when the donor reactant is more visible relative to the acceptor reactant

In the left panel of Fig. 4 *B*, the cross-correlation shape function is plotted as a function of E assuming that the visibility of acceptor reactant, B, is 15 times lower than for donor reactant, A ($\eta_A^\alpha = 15$ and $\eta_B^\beta = 1$ kHz). In this case, direct excitation of acceptor B is relatively poor (e.g., by one-photon excitation) but energy transfer from donor A can lead to sensitized emission from acceptor B. With such a visibility difference, the sensitivity of $H_{\alpha\beta}(\tau)$ to reaction kinetics is enhanced by nearly 50% for the case shown ($E = 0.9$). In the right panel of Fig. 4 *B*, the opposite case is presented in which donor *A* is 15 times dimmer than the acceptor B ($\eta_A^\alpha = 1$ and $\eta_B^\beta = 15$ kHz). Energy-transfer enhancements are significantly reduced. In general, a simple difference in the visibility of reactants (without energy transfer or a difference in reactant hydrodynamics) does *not* lead to an enhancement of reaction effects on the shape of the correlation functions.

The FRET-enhanced effects of reaction kinetics on $H_{xy}(\tau)$ can be enhanced if a hydrodynamic change accompanies reaction

In Fig. 4 *C*, the cross-correlation shape function is shown as a function of E for a system in which one reactant (and the complex) diffuses 10 times slower than the other reactant. For a hydrodynamic difference of this magnitude, reaction kinetics can have a significant effect on $H_{\alpha\beta}(\tau)$ even without energy transfer (cf. Fig. 3, *bottom*). The synergy between energy transfer and a hydrodynamic difference is greatest when the donor A is the slower diffusing reactant (Fig. 4 *C*, *left* and *right*). For an even larger difference between reactant diffusion coefficients, the influence of kinetics on $G_{\alpha\beta}(0_+)$ is further enhanced by energy transfer (Fig. 4 *D*).

Sensitivity of $G_{xy}(\tau)$ to reaction kinetics

The shape functions in Fig. 3 and 4 are exact theoretical predictions without added experimental errors. Because of the statistical nature of TCFCS, points along the correlation curve will have intrinsic errors (approximated by Eq. 19) that limit the ability to resolve reaction kinetics. To assess whether the effects of reaction kinetics on the measured correlation functions are experimentally detectable, F-statistics, F_{xy}, were computed (see Methods).

The F_{xy} statistics quantify the appropriateness of a reaction-diffusion model versus a diffusion-only model in describing the simulated correlation function data (Eq. 18). In Fig. 5, F_{xy}-contour plots are shown for the worse-case scenario $D_A = D_B = D_C$ as a function of K_d, ζ, and E, assuming a two-photon 3DG volume of $w_r = 0.48$ and $\kappa = 2.8$, $\bar{C}_A^{tot} = \bar{C}_B^{tot} = 10^{-8}$ M, $D = 8.5 \times 10^{-7}$ cm^2/s, and a total data acquisition time of 60 s. Contour plots do not change significantly if a one-photon 3DG volume of $w_r = 0.33$ and $\kappa = 5$ (e.g., Langowski and Tewes, 2000) is used (not shown). Results for equivalently visible reactants ($\eta_A^\alpha = \eta_B^\beta = 15$ kHz) are shown in Fig. 5 A and for a less visible acceptor reactant B ($\eta_A^\alpha = 15$ and $\eta_B^\beta = 1$ kHz) in Fig. 5 B; a background fluorescence of $\overline{b^\alpha} = \overline{b^\beta} = 0.45$ kHz was assumed (Eq. 2).

The gray shading denotes regions in which $F_{xy} \geq 1.3$, as demarcated by the solid contour. Using $\geq$100 correlation-function time points to compute F_{xy}, values $\geq$1.3, imply that reaction can be detected with a statistically significant p-value of $<$0.09 (see Methods). The variance for each time point along the detector correlation function, and thus the value of F_{xy}, is dependent upon the total data acquisition time, T (Eqs. 18 and 19). As acquisition time increases,

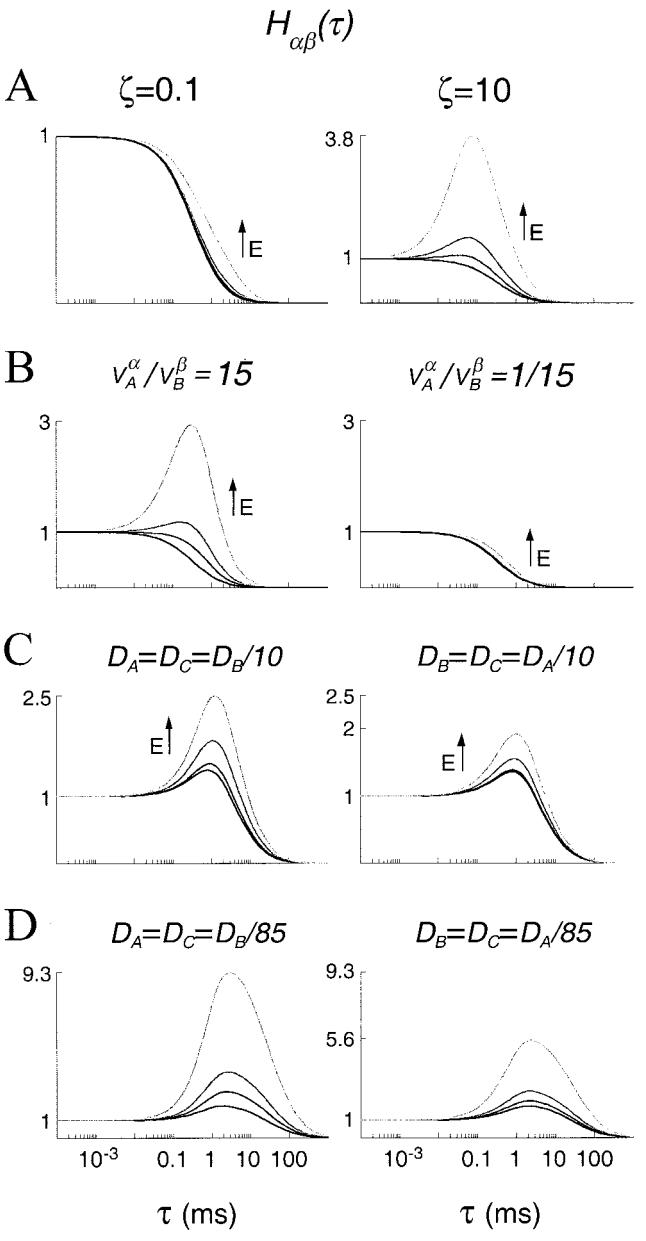

FIGURE 4 In the presence of FRET, the shape of the detector cross-correlation is sensitive to the average number of reaction turnover events observed per diffusive dwell time, the ratio of reactant visibilities, and a difference in the diffusion coefficients of reactants. (*A*) Effect of ζ, the number of reaction turnover events observed per diffusive dwell time (Eq. 15), on $H_{\alpha\beta}(\tau)$: (*left*) $\zeta = 0.1$; (*right*) $\zeta = 10$. (*B*) Effect of differential reactant visibility: (*left*) $\eta_A^\alpha = 15$ kHz and $\eta_B^\beta = 1$ kHz; (*right*) $\eta_A^\alpha = 1$ kHz and $\eta_B^\beta = 15$ kHz. (*C*) Effect of differential reactant diffusion: (*left*) $D_A = D_C = 8.5 \times 10^{-8}$ cm^2/s and $D_B = 8.5 \times 10^{-7}$ cm^2/s and (*right*) $D_B = D_C = 8.5 \times 10^{-8}$ cm^2/s and $D_A = 8.5 \times 10^{-7}$ cm^2/s. (*D*) Same as (*C*) with (*left*) $D_A = D_C = 1 \times 10^{-8}$ cm^2/s and $D_B = 8.5 \times 10^{-7}$ cm^2/s and (*right*) $D_B = D_C = 1 \times 10^{-8}$ cm^2/s and $D_A = 8.5 \times 10^{-7}$ cm^2/s. Arrows point in the direction of increasing $E = 0$, 0.5, 0.7, and 0.9. Parameters are as in Fig. 3 unless otherwise indicated.

detection sensitivity improves in a manner proportional to $\sqrt{T}$, as indicated by the dashed contour ($T = 240$ s) and the long-dashed contour ($T = 960$ s) (Fig. 5 A, *center*, *bottom*).

As energy transfer efficiency increases, a larger subset of K_d:ζ reaction conditions becomes accessible to TCFCS curve-shape analysis. As E increases, fewer reaction turnover events per diffusive dwell time are needed to observe the effects of reaction kinetics (contour boundaries shift to lower log ζ values). Consistent with the results of Fig. 3 showing that the shape of the cross-correlation function is most sensitive to E, when reactants are comparable in visibility, a larger subset of E-enhanced reactions is accessible by $G_{\alpha\beta}(\tau)$ analysis than by $G_{\alpha\alpha}(\tau)$ or $G_{\beta\beta}(\tau)$ auto-correlation analysis (Fig. 5 *A*). When $\eta_A^\alpha > \eta_B^\beta$, the subset of reactions amenable to $G_{\beta\beta}(\tau)$ and $G_{\alpha\beta}(\tau)$ analysis increases (contours shift down to lower ζ values, by about an order of magnitude) (Fig. 5 *B*). Contour boundaries are approximately parabolic in ζ, with minima centered around $\sim C_A^{tot} = C_B^{tot} = 10^{-8}$ M for the case shown. If the total concentration of reactants ($\bar{C}_A^{tot} = \bar{C}_B^{tot}$) is increased, contour boundaries shift to the right toward higher K_d by a comparable amount, though without a significant change in shape (not shown).

Determining particle concentrations by $G_{xy}(0_+)$ analysis

The magnitude of the double-detector correlation function amplitude, $G_{xy}(0_+)$, is a function of both the average number and relative visibility of particles in the probe volume, V (Eq. 13). In Fig. 6, the detector auto- and cross-correlation amplitudes in the absence of energy transfer are plotted as a function of K_d with $\bar{C}_A^{tot} = \bar{C}_B^{tot} = 10^{-8}$ M. Both detector auto-correlation function amplitudes, $G_{\alpha\alpha}(0_+)$ and $G_{\beta\beta}(0_+)$, are independent of K_d as expected according to Eq.14, because $1/G_{\alpha\alpha}(0_+) \propto (\bar{N}_A + \bar{N}_C) \propto \bar{C}_A^{tot}$ and $1/G_{\beta\beta}(0_+) \propto (\bar{N}_B + \bar{N}_C) \propto \bar{C}_B^{tot}$. In contrast, the cross-correlation function amplitude versus K_d relation is sigmoidal. Unlike the auto-correlation function amplitudes, the cross-correlation amplitude is directly proportional to the number of C molecules (Eq. 14). $G_{\alpha\beta}(0_+)$ amplitudes decrease as K_d increases above $\bar{C}_A^{tot} = \bar{C}_B^{tot}$ ($\Gamma \rightarrow 1$ and reaction equilibrium favors reactants, Eq. 16). As K_d decreases below $\bar{C}_A^{tot} = \bar{C}_B^{tot}$ (equilibrium favors the formation of C), the cross-correlation amplitude approaches an asymptotic value corresponding to $\bar{C}_C \rightarrow \bar{C}_A^{tot} = \bar{C}_B^{tot}$.

Energy transfer results in lower cross-correlation amplitudes, $G_{\alpha\beta}(0_+)$

As energy transfer efficiency increases, both α- and β-detector auto-correlation amplitude curves increase in a complicated fashion as governed by Eq. 13 (Fig. 7 *A*). The cross-correlation function amplitude, $G_{\alpha\beta}(0_+)$, is proportional to $r_C^\alpha r_C^\beta$. Using Eq. 12 and assuming equivalently visible reactants, $r_C^\alpha r_C^\beta = (1 - E)(1 + E)$, which is a parabolic function in energy-transfer efficiency having a maximum at $E = 0$. Thus, as E increases, $G_{\alpha\beta}(0_+)$ ampli-

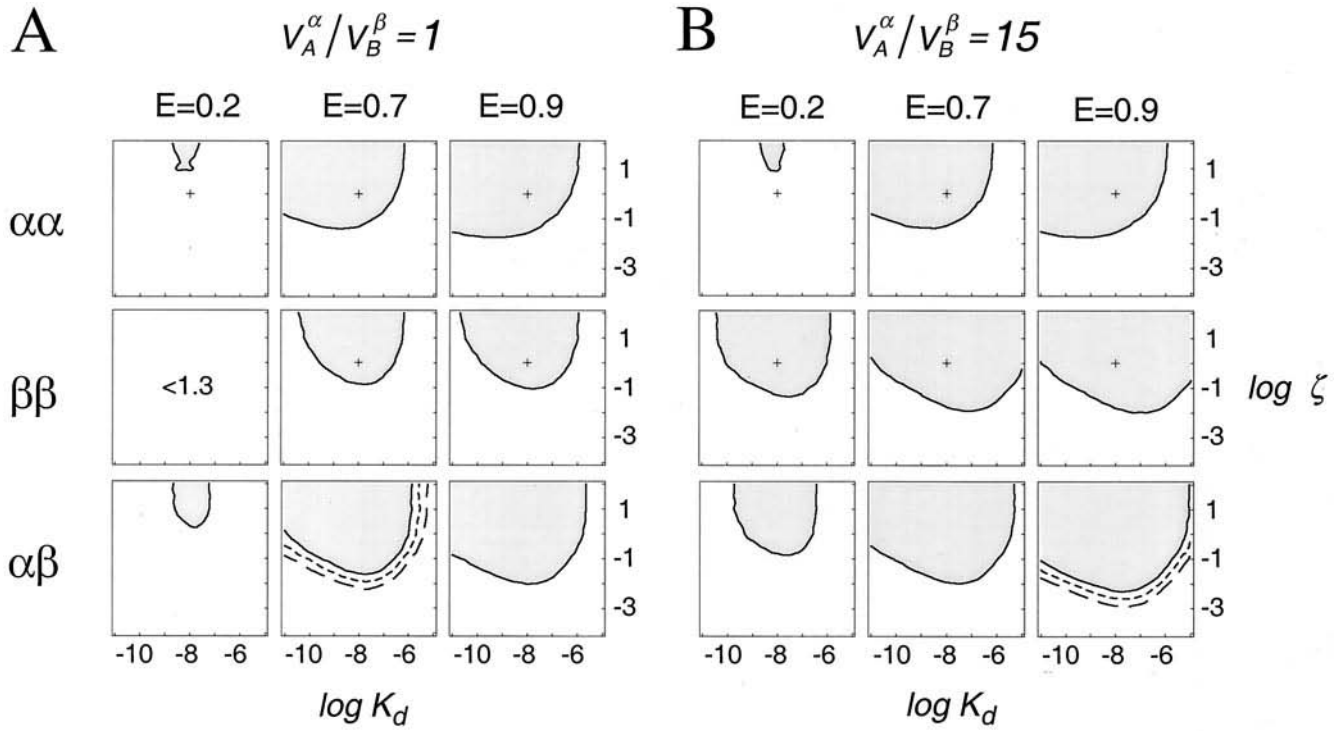

FIGURE 5 Limits of detector correlation function sensitivity to reaction. Contour plots of F_{xy} as a function of E. F_{xy} characterizes the feasibility of discriminating between the detector correlation functions (Eqs. 9 and 10) expected for a diffusion-only system (A, B, C) versus a reaction-diffusion system (A + B ↔ C) (Eq. 18). Solid contour lines demarcate regions (*gray*) in which the presence of reaction can be detected with a confidence level of $p < 0.09$ using a data-acquisition time of 60 s (see Methods). Detection sensitivity is improved in a manner proportional to the square root of the data-acquisition time (Eq. 19) as indicated by the dashed contour (240 s) and long-dashed contour (960 s). Parameters: $\bar{C}_A^{tot} = \bar{C}_B^{tot} = 10^{-8}$ M, $w_r = 0.48$ μm, $r_B^\alpha = r_A^\beta = 0$, $\kappa = 2.8$, $\bar{b}^\alpha = \bar{b}^\beta = 0.45$ kHz (Eq. 2), and (*A*) $\eta_A^\alpha = \eta_B^\beta = 15$ kHz; or (*B*) $\eta_A^\alpha = 15$ kHz, $\eta_B^\beta = 1$ kHz. The cross-hair marks the condition in which $\bar{C}_A^{tot} = \bar{C}_B^{tot} = K_d$, with one reaction turnover event observed on average per diffusive dwell time (log $\zeta = 0$). Contours shift to the right as $\bar{C}_A^{tot} = \bar{C}_B^{tot}$ increases (see text).

tudes decrease for all values of K_d (Fig. 7 B). The right panel of Fig. 7 *B* shows an expanded view in the region where cross-correlation amplitudes drop below the statistical noise/detection limits indicated by the dashed (T = 240 s) and long-dashed $T = 960$ s) lines. For the case shown ($\bar{C}_A^{tot} = \bar{C}_B^{tot} = 10^{-8}$ M), with $T = 240$ s and $E = 0.9$ or $T =$ 960 s and $E = 0.7$, the maximum K_d that yields a cross-correlation amplitude greater than the estimated statistical error is $K_d^{max} \sim 10^{-6}$ M. For $\bar{C}_A^{tot} = \bar{C}_B^{tot} = 10^{-7}$ M under similar conditions, $K_d^{max} \sim 10^{-5}$ M (not shown). In general, the maximum K_d that leads to a measurable cross-correlation amplitude above statistical noise is given by $K_d^{max} \sim (\bar{C}_A^{tot} = \bar{C}_B^{tot}) \cdot 10^2$.

DISCUSSION

Energy transfer in TCFCS

The motivations for this study were two-fold: 1) to assess the utility of TCFCS for studying reversible bimolecular reactions without the need for reaction initiation or chemical perturbation, and 2) to determine the influence of resonance energy transfer on TCFCS auto- and cross-correlation functions. The results presented in Fig. 7 indicate that determination of particle concentrations via $G_{xy}(0_+)$ amplitude analysis is complicated by FRET (Eq. 14 and Appendix C). Moreover, the presence of FRET produces decreased detector cross-correlation amplitudes. If $E < 0.3$, the effects of FRET on $G_{xy}(0_+)$ can generally be ignored, and particle concentrations can be determined using Eq. 14 to within an error of ≤10%. As mean energy transfer efficiencies increase above $E = 0.3$, the error increases exponentially.

Although FRET complicates $G_{xy}(0_+)$ analysis and is best avoided if only particle concentrations (or ratios) are of interest, FRET is advantageous for measurements of bimolecular reaction kinetics. If reaction components are of comparable size, reaction kinetics cannot be detected without FRET. Our results suggest that, under certain conditions, TCFCS in conjunction with FRET can be used to monitor reaction kinetics. The interplay between energy transfer and reaction kinetics in altering the shape of the correlation function as proposed here has been demonstrated recently in a different context by Widengren et al. (2001). In contrast to our results (which assess the possibility of measuring reaction kinetics given a known amount

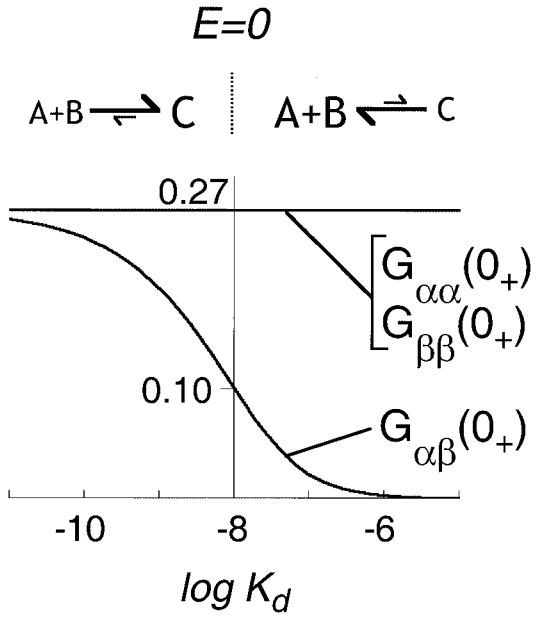

FIGURE 6 Detector correlation function amplitudes as a function of the dissociation constant for the reaction A + B $\underset{k_b}{\overset{k_f}{\longleftrightarrow}}$ C. $G_{xy}(0_+)$ amplitudes computed assuming zero energy transfer (Eq. 15). Parameters: $\bar{C}_A^{tot} = \bar{C}_B^{tot} = K_d = 10^{-8}$ M, $w_r = 0.48$ μm, $\kappa = 2.8$, $\eta_A^\alpha = \eta_B^\beta = 15$ kHz, and zero background fluorescence.

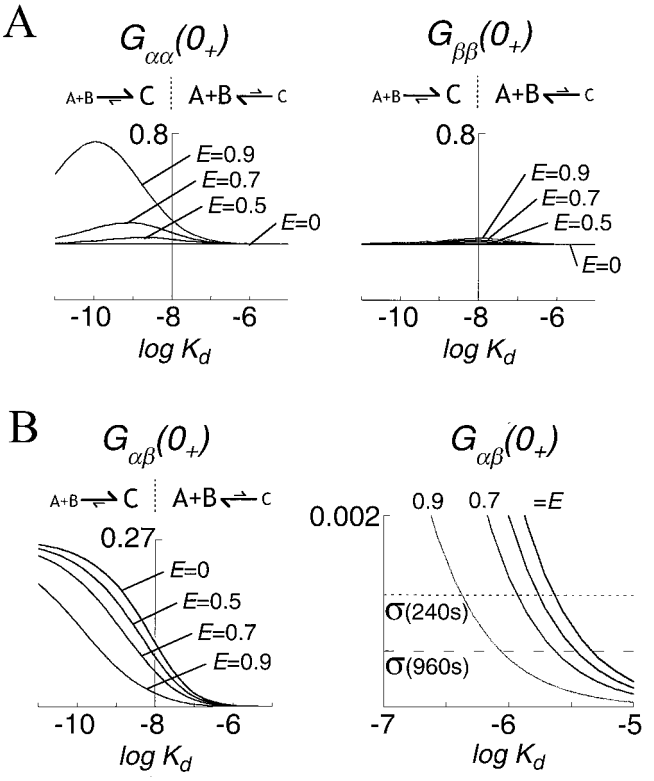

FIGURE 7 Detector correlation function amplitudes are sensitive to energy transfer. Detector auto-correlation (*A*) and cross-correlation (*B*) amplitudes versus log K_d as a function of E (Eq. 13). (*B, right*) Expanded view in the region where cross-correlation amplitudes are comparable to the experimental amplitude errors assuming data acquisition times of 240 or 960 s (*dashed lines*). Parameters are as in Fig. 6.

of energy transfer), Widengren et al. exploited the effects of a fluorophore cis–trans isomerization reaction on the shape of the auto-correlation function as a means to measure FRET efficiencies of double-labeled DNA duplexes of varying lengths.

Analysis of bimolecular reaction kinetics by TCFCS

To successfully measure reaction kinetics by curve-shape analysis, a sufficient number of "reaction fluctuations" per observation interval, ζ, must be observed. The dimensionless parameter ζ is a function of the characteristic diffusion time of the reacting particles in the probe volume, τ_{diff}, the position of equilibrium variable, Γ, and the reverse rate constant, k_b (Eq. 15). For unimolecular reactions, $\Gamma = 1 + k_f/k_b$, and ζ is a function of the forward and reverse rate constants but not reactant concentrations. For bimolecular reactions, however, Γ and thus ζ are functions of k_f and k_b, as well as the equilibrium constant for the reaction relative to the total concentration of the reactants (see Eq. 16). When $\bar{C}_A^{tot} = \bar{C}_B^{tot}$, the relative concentration fluctuations for both the reactants *and* complex are greatest (Bernasconi, 1976), leading to maximal detector cross-correlation function amplitudes.

From the $G_{xy}(\tau)$ reaction sensitivity landscapes in Fig. 5, the reaction conditions that permit measurable differences in the detector correlation functions can be determined. For a two-photon 3DG volume of $w_r = 0.48$ μm and $\kappa = 2.8$, with $D_A = D_B = D_C = 8.5 \times 10^{-7}$ cm^2/s (D for green fluorescent protein in water, Dayel et al., 1999), $\tau_{diff} \sim (3.7 \times 10^{-4}\ s)$; this value is similar for a one-photon 3DG with $w_r = 0.33$ μm and $\kappa = 5$. Using Eq. 15, $\zeta = \tau_{diff} k_f K_d/\Gamma$, and expressing Γ as a function of $\bar{C}_A^{tot}$, $\bar{C}_B^{tot}$, and K_d (Eq. 16), the conditions under which reactions are accessible by $G_{\alpha\beta}(\tau)$ analysis can be estimated from the contours of Fig. 5. These reaction conditions are shown in Fig. 8 assuming $E = 0.9$, $T = 960$ s, and $\eta_A^\alpha/\eta_B^\beta = 15$, for different values of $\bar{C}_A^{tot} = \bar{C}_B^{tot}$. For reactions with a $K_d \sim 10^{-9}$ M, reaction kinetics are typically inaccessible unless $k \geq \sim 10^9$ M^{-1}s^{-1}. Reactions with $k_f \geq \sim 10^8$ M^{-1}s^{-1} are accessible if the K_d is within the window of $\sim 10^{-8}$ to $\sim 10^{-6}$ M, for all the total reactant concentrations shown (*dark gray*). As $\bar{C}_A^{tot} = \bar{C}_B^{tot}$ increases, lower affinity reactions with slower forward rates can be studied: if $\bar{C}_A^{tot} = \bar{C}_B^{tot} = 10^{-7}$ M, reactions with a $K_d \leq 10^{-5}$ M and $k_f \geq \sim 10^7$ M^{-1}s^{-1} are accessible; if $\bar{C}_A^{tot} = \bar{C}_B^{tot} = 10^{-6}$ M, reactions with a $K_d \leq 10^{-4}$ M and $k \geq \sim 10^6$ M^{-1}s^{-1} should be accessible. To optimize the influence of kinetics on the detector cross-correlation function, the reactive system is best poised when $K_d \times 10^{-2} \leq (\bar{C}_A^{tot} = \bar{C}_B^{tot}) \leq K_d \times 10^2$,

where the upper limit ensures that $G_{xy}(0_+)$ amplitudes are measurable above statistical noise.

The resolution of reaction kinetics by $G_{xy}(\tau)$ analysis can also be improved if other reactant property differences exist or these properties change upon reaction. As demonstrated in Fig. 4 *C* and 4 *D*, if the diffusion coefficient for one reactant is significantly larger than the other, the influence of kinetics on $G_{\alpha\beta}(0_+)$ can be observed without the presence of energy transfer, although energy transfer magnifies these effects. A significant quantum yield change of one reactant upon binding could also result in a pronounced effect of reaction on $G_{xy}(\tau)$. This has been demonstrated in studies of ethidium bromide binding to DNA (Elson and Magde, 1974; Magde et al., 1974; Icenogle and Elson, 1983) and of 1-anilino-8-naphthalene sulfonic acid binding to partially folded proteins (Lamb et al., 2000; Bismuto et al., 2001). Quantum yield enhancement upon binding in combination with FRET would likely extend the set of reactions accessible to TCFCS analysis.

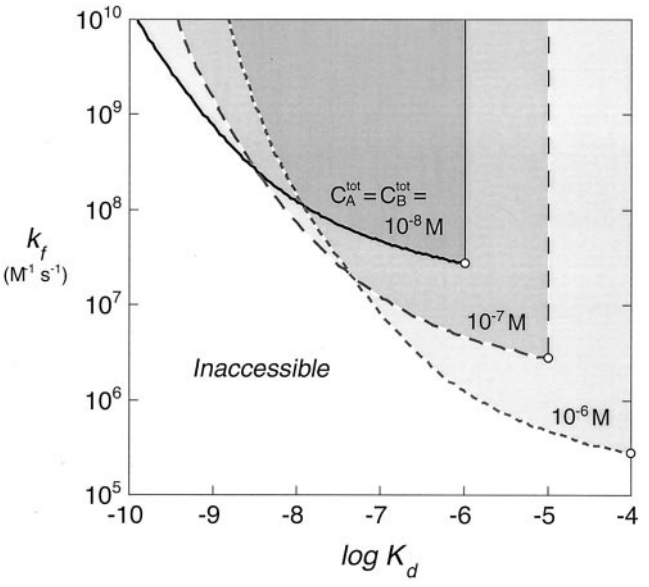

FIGURE 8 Subset of bimolecular reaction kinetics accessible to detector cross-correlation function analysis. Subset of reaction parameters (k_f, K_d, and $\bar{C}_A^{tot} = \bar{C}_B^{tot}$ that lead to measurable differences in $G_{\alpha\beta}(\tau)$ ($F_{\alpha\beta} \geq 1.3$) indicated in different tones of gray and determined from Fig. 5 using $\zeta \sim \tau_{diff}\, k_f K_d/\Gamma$ (Eqs. 15 and 16) with $\tau_{diff} \sim 3.7 \times 10^{-4}$ s, for $E = 0.9$, $T = 960$ s, and $\eta_A^\alpha/\eta_B^\beta = 15$. Open circles mark the condition, $K_d = (\bar{C}_A^{tot} = \bar{C}_B^{tot}) \times 10^2$, an estimate of the maximum K_d with detectable $G_{\alpha\beta}(0_+)$ amplitudes above statistical noise. Shown for $\bar{C}_A^{tot} = \bar{C}_B^{tot} = 10^{-8}$ M (*solid line*), 10^{-7} M (*dashed*), and 10^{-6} M (*short dashed*).

Biochemical relevance

The association rate for two molecules can be expressed as $k_f = p_{bind} \cdot k_{coll}$, where k_{coll} is the diffusional encounter rate and p_{bind} is the probability of successful binding upon colliding. From simple collision theory, $k_{coll} \sim 7 \times 10^{-9}$ $M^{-1}s^{-1}$ in water for comparably sized reactants; if one reactant is larger than the other, k_{coll} may be higher due to the larger target area of the former and higher mobility of the latter (Fersht, 1999). For protein–protein complexes, p_{bind} is typically $\sim 10^{-5}$ (Janin, 2000) and basal protein–protein docking rates in vitro are $\sim 10^5$ $M^{-1}s^{-1}$, although long-range electrostatic factors can accelerate these rates by up to 10^3 (Northrup and Erickson, 1992; Schreiber and Fersht, 1996; Janin, 1997). Thus, association rates constants, k_f, for protein complexes typically are in the range 10^4–10^8 $M^{-1}s^{-1}$, with the majority $\sim 10^6$ $M^{-1}s^{-1}$ (Northrup and Erickson, 1992; Fersht, 1999; Janin, 2000; Gabdoulline and Wade, 2001). Dissociation rates are much more varied, typically in the range 10^{-7}–10^4 s^{-1} (Fersht, 1999; Janin, 2000), so that K_d are in the range 10^{-13}–10^{-2} M. Protein–ligand (e.g., antibody–hapten) and small nucleic-acid duplex interactions generally have faster association and dissociation rates (10^7–10^9 $M^{-1}s^{-1}$ and 10^1–10^4 s^{-1}, respectively), with K_d typically spanning the range 10^{-8}–10^{-3} M (Pecht and Lancet, 1977; Cantor and Schimmel, 1980; Fersht, 1999).

The results of the analysis here suggest that the kinetic rate constants for a subset of these protein–protein and protein–ligand reactions can be deduced by curve-shape analysis of the detector cross-correlation function, provided energy transfer efficiency within the reaction complex is sufficiently high ($E \geq 0.7$), a sufficient experimental data acquisition time, the total concentration of reactants is sufficiently high ($\geq 10^{-8}$ M), and the reaction equilibrium is properly poised. When reactants are comparably sized, reactions must typically be near the diffusion-limit ($k \geq 10^7$ $M^{-1}s^{-1}$) to be observable. Examples of macromolecular interactions characterized by very fast association rates include: barnase and barstar (10^8–10^{10} $M^{-1}s^{-1}$; Schreiber and Fersht, 1996), insulin dimerization (10^8 $M^{-1}s^{-1}$; Koren and Hammes, 1976), cytochrome *c* with cytochrome *c* peroxidase or cytochrome b5 (10^7–10^9 $M^{-1}s^{-1}$; Northrup and Erickson, 1992), various tRNA and tRNA synthetases (10^8 $M^{-1}s^{-1}$; Fersht, 1999), and unfolded bovine pancreatic trypsin inhibitor and the *E. coli* chaperone SecB (10^9–10^{10} $M^{-1}s^{-1}$; Fekkes et al., 1995). When one reactant is considerable larger than the other reactant, the subset of kinetic parameters that lead to detectable changes in the cross-correlation function is extended. Some biological examples where reactants have very different diffusion coefficients include the binding of cytosolic proteins to membrane proteins, lipidic domains, or scaffold proteins (Faux and Scott, 1996; Hurley and Meyer, 2001), and of soluble factors to relatively immobile cytoskeletal or vesicular structures.

In summary, it should be possible to study a subset of biologically relevant bimolecular reactions by analysis of TCFCS correlation functions without the need for chemical perturbation. Although $G_{xy}(0_+)$ analysis of reactant concentrations is substantially complicated by the presence of energy transfer, FRET is advantageous for kinetic studies, and essential if there is little hydrodynamic difference between interacting components. If particle concentrations are the primary

quantities of interest, the effects of FRET may be neglected for $E \leq 0.3$ without incurring significant error ($\leq$10%).

APPENDIX A

For the bimolecular reaction,

$$A + B \underset{k_b}{\overset{k_f}{\leftrightarrow}} C,$$

the linearized reaction-diffusion matrix Eq. 4 is

$$\mathbf{M} = \begin{bmatrix} k_f\bar{C}_B - D_A\mathbf{q}^2 & -k_f\bar{C}_A & k_b \\ -k_f\bar{C}_B & -k_f\bar{C}_A - D_B\mathbf{q}^2 & k_b \\ k_f\bar{C}_B & k_f\bar{C}_A & -k_f - D_c\mathbf{q}^2 \end{bmatrix}. \tag{A1}$$

By detailed balance ($R_{ij}C_j = R_{ji}C_i$), $\mathbf{M}$ can be made symmetric by the similarity transformation $\mathbf{M}_{sym} = \mathbf{X}^{-1}\mathbf{M}\mathbf{X}$, where $\mathbf{X}$ is the diagonal matrix with $\mathbf{X}_{ij} = \sqrt{\bar{C}_i}\delta_{ij}$ (Elson and Magde, 1974; Icenogle 1981; Wei and Prater, 1962). Using the following reduced variables, $\rho = k_b/D_c$, $\theta_A = \bar{C}_A/\bar{C}_C$, $\theta_B = \sqrt{\bar{C}_B/\bar{C}_C}$, $\theta_C = -1$, $\hat{D}_A = D_A/D_C$, and $\hat{D}_B = D_B/D_C$, the matrix $\mathbf{M}_{sym}$ becomes

$$\mathbf{M}_{sym} = \rho D_C \cdot \begin{bmatrix} -1/\theta_A^2 - \hat{D}_A\mathbf{q}^2/\rho & -1/(\theta_A\theta_B) & 1/\theta_A \\ -1/(\theta_A\theta_B) & -1/\theta_B^2 - \hat{D}_B\mathbf{q}^2/\rho & 1/\theta_B \\ 1/\theta_A & 1/\theta_B & -1/\theta_C^2 - \mathbf{q}^2/\rho \end{bmatrix}. \tag{A2}$$

Solutions to Eq. 4 for $\delta\bar{\mathbf{C}}(\mathbf{q}, \tau)$ are obtained by solving for the eigenvalues and eigenfunctions of $\mathbf{M}_{sym}$. The spatio-temporal dissipation function $Z_{ij}(\mathbf{q}, \tau)$ in Eq. 7 can then be written as: $Z_{ij}(\mathbf{q}, \tau) = \Sigma_s\, Y_j^{(s)} \cdot \exp[\lambda(s)\tau] \cdot Y_i^{-1(s)}$, where $Y^{(s)}$ and $Y^{-1(s)}$ are the sth eigenvector and inverse eigenvector, respectively, corresponding to the eigenvalue $\lambda^{(s)}$ (Elson and Magde, 1974; Icenogle, 1981). Use of a symmetric matrix leads to six unique Z_{ij} ($= Z_{ji}$) expressions rather than eight if the matrix $\mathbf{M}$ were used directly (for which $Z_{ij} \neq Z_{ji}$).

For the bimolecular reaction,

$$A + B \underset{k_b}{\overset{k_f}{\leftrightarrow}} C,$$

with $\hat{D}_A = \hat{D}_B = 1$, the diffusive and reactive components of $Z_{ij}(\mathbf{q}, \tau)$ decouple

$$Z_{ij}(\mathbf{q}, \tau) = \exp[-(w_r^2\mathbf{q}^2\tau/4n_p\tau_{diff})] \times [\delta_{ij} + \Gamma(\exp(-r/\tau_{reac} - 1))/\theta_i\theta_j], \tag{A3}$$

where Γ is defined in association with Eq. 16. With $\hat{D}_A = 1$ and $\hat{D}_B \gg 1$, the $Z_{ij}(\mathbf{q}, \tau)$ functions are

$$Z_{AA}(\mathbf{q}, \tau) = \left(\frac{1}{1 + 1/\theta_A^2}\right) \times \left(E_{diff} + \frac{E_{reac}}{\theta_A^2}(C - (1 + \mathbf{q}^2T - Q)S)\right),$$

$$Z_{BB}(\mathbf{q}, \tau) = E_{reac}(C + (1 + \mathbf{q}^2T - Q)S),$$

$$Z_{CC}(\mathbf{q}, \tau) = \left(\frac{1}{1 + 1/\theta_A^2}\right) \times \left(\frac{E_{diff}}{\theta_A^2} + E_{reac}(C - (1 + \mathbf{q}^2T - Q)S)\right),$$

$$Z_{AB}(\mathbf{q}, \tau) = -\left(\frac{\theta_B}{\theta_A}\right) E_{reac}(Q\,S),$$

$$Z_{BC}(\mathbf{q}, \tau) = \theta_B\, E_{reac}(Q\,S),$$

$$Z_{AC}(\mathbf{q}, \tau) = \left(\frac{1}{\theta_A + 1/\theta_A}\right) \times (E_{diff} - E_{reac}(C - (1 + \mathbf{q}^2T - Q)S)), \tag{A4}$$

$$E_{diff} = \exp\left[-\left(\frac{w_r^2\mathbf{q}^2}{4n_p}\right)\frac{\tau}{\tau_C}\right],$$

$$E_{reac} = \exp\left[-\left(\frac{1 + \mathbf{q}^2P}{2}\right)\frac{\tau}{\tau_{reac}}\right],$$

$$C = \cosh\left[\frac{U(\mathbf{q}^2)\tau}{2\tau_{reac}}\right], \qquad S = \sinh\left[\frac{U(\mathbf{q}^2)\tau}{2\tau_{reac}}\right] \Big/ U(\mathbf{q}^2),$$

$$U(\mathbf{q}^2) = \sqrt{(1 + \mathbf{q}^2L)^2 - 2\mathbf{q}^2LQ}, \qquad Q = 2\Gamma/\theta_B^2,$$

$$L = D_C(1 - \hat{D}_B)\tau_{reac}, \qquad P = D_C(1 + \hat{D}_B)\tau_{reac},$$

$$\tau_C = \frac{w_r^2}{4n_pD_C}.$$

For $D_A \neq D_B \neq D_C$, the eigenvalues and eigenvectors for $\mathbf{M}_{sym}$ (Eq. A2) must be solved using a modified cubic root equation assuming real roots (Weisstein, 1999). The resulting $Z_{ij}(\mathbf{q}, \tau)$ functions are available for download at: http://www.ucsf.edu/verklab/erik/generalZfunctions.pdf.

APPENDIX B

The double-detector correlation functions of Eq. 5 can be written explicitly and generally as

$$G_{\alpha\alpha}(\tau) = \left(\frac{\aleph_\alpha^2}{\bar{N}_A}\right)\left(\frac{\theta_A^2}{(\theta_A^2 + r_B^\alpha\theta_B^2 + r_C^\alpha\theta_C^2)^2}\right) \times \left[\begin{array}{l}\theta_A^2h_{AA}(\tau) + (r_B^\alpha)^2\,\theta_B^2h_{BB}(\tau) + (r_C^\alpha)^2\,\theta_C^2h_{CC}(\tau) \\ \quad + 2r_B^\alpha\theta_A\theta_Bh_{AB}(\tau) - 2r_C^\alpha\theta_A\theta_Ch_{AC}(\tau) - 2r_B^\alpha r_C^\alpha\theta_B\theta_Ch_{BC}(\tau)\end{array}\right],$$

$$G_{\beta\beta}(\tau) = \left(\frac{\aleph_\beta^2}{\bar{N}_B}\right)\left(\frac{\theta_B^2}{(r_A^\beta\theta_A^2 + \theta_B^2 + r_C^\beta\theta_C^2)^2}\right) \times \left[\begin{array}{l}(r_A^\beta)^2\theta_A^2h_{AA}(\tau) + \theta_B^2h_{BB}(\tau) + (r_C^\beta)^2\theta_C^2h_{CC}(\tau) \\ \quad + 2r_A^\beta\theta_A\theta_Bh_{AB}(\tau) - 2r_A^\beta r_C^\beta\theta_A\theta_Ch_{AC}(\tau) - 2r_C^\beta\theta_B\theta_Ch_{BC}(\tau)\end{array}\right],$$

$$G_{\alpha\beta} = \left(\frac{\aleph_\alpha\aleph_\beta}{\bar{N}_C}\right)\left(\frac{\theta_C^2}{(\theta_A^2 + r_B^\alpha\theta_B^2 + r_C^\alpha\theta_C^2)\,(r_A^\beta\theta_A^2 + \theta_B^2 + r_C^\beta\theta_C^2)}\right) \times \left[\begin{array}{l}r_A^\beta\theta_A^2h_{AA}(\tau) + r_B^\alpha\theta_B^2h_{BB}(\tau) + r_C^\alpha r_C^\beta\theta_C^2h_{CC}(\tau) \\ \quad + (1 + r_B^\alpha r_A^\beta)\theta_A\theta_Bh_{AB}(\tau) - (r_C^\beta + r_C^\alpha r_A^\beta)\theta_A\theta_Ch_{AC}(\tau) \\ \qquad\qquad - (r_B^\alpha r_C^\beta + r_C^\alpha)\theta_B\theta_Ch_{BC}(\tau)\end{array}\right], \tag{B1}$$

where $r_B^\alpha = \eta_B^\alpha/\eta_A^\alpha$ and $r_A^\beta = \eta_A^\beta/\eta_B^\beta$ are conjugate variables that describe the amount of nonideal bleed-through fluorescence registered in a nonpreferred detector channel. When $r_A^\beta = r_B^\alpha = 0$, the expressions of Eq. B1 simplify to those of Eqs. 9 and 10.

The relative α- and β-visibilities for the complex C, formed by the association of donor A and acceptor B, can be written in terms of intended and bleedthrough contributions as

$$\begin{aligned} r_C^\alpha = \frac{\eta_C^\alpha}{\eta_A^\alpha} &= \underbrace{(1-E)}_{\text{intended}} + \underbrace{\left\{\frac{r_B^\alpha \eta_B^\beta}{\eta_A^\alpha}\left(1+\left[\frac{\Phi_B \eta_A^\alpha}{\eta_B^\beta}\right]E\right)\right\}}_{\text{bleedthrough}}, \\ r_C^\beta = \frac{\eta_C^\beta}{\eta_B^\beta} &= \left(1+\left[\frac{\Phi_B \eta_A^\alpha}{\eta_B^\beta}\right]E\right) + \left\{\frac{r_A^\beta \eta_A^\alpha}{\eta_B^\beta}(1-E)\right\} \end{aligned} \quad \text{(B2)}$$

where Φ_B is the product of the quantum yield for acceptor species B (Q_B) and the ratio of the β to α channel detection efficiencies (g_β/g_α). When $\Phi_B = 1$ and $r_A^\beta = r_B^\alpha = 0$, Eq. B2 simplifies to Eq. 12.

APPENDIX C

Expressions for $\bar{N}_A$, $\bar{N}_B$, and $\bar{N}_C$ as a function of $G_{\alpha\alpha}(0_+)$, $G_{\beta\beta}(0_+)$, and $G_{\alpha\beta}(0_+)$ for the case in which there is no bleedthrough fluorescence:

$$\begin{aligned} \bar{N}_A &= (r_C^\alpha)^2\,(r_C^\beta \aleph_\alpha G_{\alpha\alpha}(0_+)G_{\beta\beta}(0_+) - (r_C^\beta - 1)\aleph_\alpha G_{\alpha\beta}^2(0_+) \\ &\quad - \aleph_\beta G_{\alpha\alpha}(0_+)G_{\alpha\beta}(0_+)) \\ &\quad \times \frac{(r_C^\beta \aleph_\alpha G_{\beta\beta}(0_+) + (r_C^\alpha - 1)\aleph_\beta G_{\alpha\beta}(0_+))}{((r_C^\alpha - 1)\,(r_C^\beta - 1)G_{\alpha\beta}^2(0_+) - r_C^\alpha r_C^\beta G_{\alpha\alpha}(0_+)G_{\beta\beta}(0_+))^2}, \\ \bar{N}_B &= (r_C^\beta)^2\,(r_C^\alpha \aleph_\beta G_{\alpha\alpha}(0_+)G_{\beta\beta}(0_+) - (r_C^\alpha - 1)\aleph_\beta G_{\alpha\beta}^2(0_+) \\ &\quad - \aleph_\alpha G_{\beta\beta}(0_+)G_{\alpha\beta}(0_+)) \\ &\quad \times \frac{(r_C^\alpha \aleph_\beta G_{\alpha\alpha}(0_+) + (r_C^\beta - 1)\aleph_\alpha G_{\alpha\beta}(0_+))}{\aleph_\beta((r_C^\alpha - 1)\,(r_C^\beta - 1)G_{\alpha\beta}^2(0_+) - r_C^\alpha r_C^\beta G_{\alpha\alpha}(0_+)G_{\beta\beta}(0_+))^2}, \\ \bar{N}_C &= G_{\alpha\beta}(0_+)\,(r_C^\alpha \aleph_\beta G_{\alpha\alpha}(0_+) - (r_C^\beta - 1)\aleph_\alpha G_{\alpha\beta}(0_+)) \\ &\quad \times \frac{(r_C^\beta \aleph_\alpha G_{\beta\beta}(0_+) + (r_C^\alpha - 1)\aleph_\beta G_{\alpha\beta}(0_+))}{((r_C^\alpha - 1)\,(r_C^\beta - 1)G_{\alpha\beta}^2(0_+) - r_C^\alpha r_C^\beta G_{\alpha\alpha}(0_+)G_{\beta\beta}(0_+))^2}. \end{aligned} \quad \text{(C1)}$$

NOTES

1. An expression equivalent to Eq. 12 of Meseth et al. (1999) is obtained by multiplying Eq. 19 by $G_{xy}(0_+)$ and substituting $(\Delta t/T) = 1/M$, $\Delta t = \Delta\tau$, $\tau_i/\Delta t = m$, $H_{xy} = g$, $G_{xy}(0_+) = 1/N$, and $\sqrt{\langle n_x\rangle\langle n_y\rangle} = \langle n\rangle$. An expression similar to Eq. 47 of Kask et al. (1997) may be obtained by substituting: $T = U$, $\Delta t = T$, and $R =$ parenthetical terms; Kask et al.'s terms in $1/m$ have been omitted here assuming $m \gg 1$, where m is the average number of particles in the probe volume that contribute to the mean fluorescence intensity in each channel.

2. For $D_A = D_B = D_C$, the maximum in $H_{\alpha\beta}(\tau)$ occurs at

$$\tau_{max} \approx \tau_{reac}(|W_{-1}[\exp(-A(1+\tau_{diff}/\tau_{reac}))]|-1)-\tau_{diff},$$

where

$$A = 1 - \sum_i^m d_{ii} \Big/ \left(\sum_i^m \sum_j^m d_{ij}\,\Gamma/\theta_i\theta_j\right)$$

and $W_{-1}[x]$ is the nonprincipal, real-branch Lambert W-function that can be approximated by $W_{-1}[x] = L_1 - L_2 + L_1/L_2$ with $L_1 = \ln[-x]$ and $L_2 = \ln[-L_1]$.

We thank Dr. Sudipta Maiti, J. Balaji, and Parijat Sengupta for helpful discussions and suggestions on FCS theory and implementation, and Dr. N. Periasamy and the Maiti Lab for hosting E.H. during a summer visit to the Tata Institute for Fundamental Research. E.H. thanks Elliot Elson for providing a copy of R. Icenogle's thesis and Andrew Tan for comments on the manuscript.

This work was supported by National Institute of Health grant EB00415. E.H. is supported in part by a predoctoral fellowship from the American Heart Association, Western States Affiliates.

REFERENCES

Bernasconi, C.F. 1976. Relaxation Kinetics. Academic Press, New York. 76–97.

Bevington, P.R., and D.K. Robinson. 1992. Data Reduction and Error Analysis for the Physical Sciences. McGraw Hill, New York.

Bismuto, E., E. Gratton, and D. C. Lamb. 2001. Dynamics of ANS binding to tuna apomyoglobin measured with fluorescence correlation spectroscopy. *Biophys. J.* 81:3510–3521.

Bonnet, G., O. Krichevsky, and A. Libchaber. 1998. Kinetics of conformational fluctuations in DNA hairpin-loops. *Proc. Natl. Acad. Sci. U.S.A.* 95:8602–8606.

Cantor, C. R., and P. R. Schimmel. 1980. Biophysical Chemistry. Part III: The Behavior of Biological Macromolecules. W. H. Freeman and Company, New York. 921, 1217.

Chandler, D. 1987. Introduction to Modern Statistical Mechanics. Oxford University Press, New York. 242–246.

Chen, Y., J. D. Müller, P. T. So, and E. Gratton. 1999. The photon counting histogram in fluorescence fluctuation spectroscopy. *Biophys. J.* 77: 553–567.

Chen, Y., J. D. Müller, S. Y. Tetin, J. D. Tyner, and E. Gratton. 2000. Probing ligand protein binding equilibria with fluorescence fluctuation spectroscopy. *Biophys. J.* 79:1074–1084.

Dayel, M. J., E. F. Hom, and A. S. Verkman. 1999. Diffusion of green fluorescent protein in the aqueous-phase lumen of endoplasmic reticulum. *Biophys. J.* 76:2843–2851.

Elson, E. L., and D. Magde. 1974. Fluorescence correlation spectroscopy. I. Conceptual basis and theory. *Biopolymers.* 13:1–27.

Faux, M. C., and J. D. Scott. 1996. Molecular glue: kinase anchoring and scaffold proteins. *Cell.* 85:9–12.

Fekkes, P., T. den Blaauwen, and A. J. Driessen. 1995. Diffusion-limited interaction between unfolded polypeptides and the *Escherichia coli* chaperone SecB. *Biochemistry.* 34:10078–10085.

Fersht, A. 1999. Structure and Mechanism in Protein Science: A Guide to Enzyme Catalysis and Protein Folding. W. H. Freeman and Company, New York. 153, 158–168.

Gabdoulline, R. R., and R. C. Wade. 2001. Protein–protein association: investigation of factors influencing association rates by Brownian dynamics simulations. *J. Mol. Biol.* 306:1139– 1155.

Geerts, H. 1983. Experimental realization and optimalization of a fluorescence correlation spectroscopy apparatus. *J. Biochem. Biophys. Methods.* 7:255–261.

Haupts, U., S. Maiti, P. Schwille, and W. W. Webb. 1998. Dynamics of fluorescence fluctuations in green fluorescent protein observed by fluorescence correlation spectroscopy. *Proc. Natl. Acad. Sci. U.S.A.* 95: 13573–13578.

Heikal, A. A., S. T. Hess, G. S. Baird, R. Y. Tsien, and W. W. Webb. 2000. Molecular spectroscopy and dynamics of intrinsically fluorescent proteins: coral red (dsRed) and yellow (Citrine). *Proc. Natl. Acad. Sci. U.S.A.* 97:11996–12001.

Heinze, K. G., A. Koltermann, and P. Schwille. 2000. Simultaneous two-photon excitation of distinct labels for dual-color fluorescence crosscorrelation analysis. *Proc. Natl. Acad. Sci. U.S.A.* 97:10377–10382.

Hurley, J. H., and T. Meyer. 2001. Subcellular targeting by membrane lipids. *Curr. Opin. Cell. Biol.* 13:146–152.

Icenogle, R. D. 1981. Fluorescence correlation spectroscopy and fluorescence photobleaching recovery studies of the binding of ethidium to deoxyribonucleic acid. Ph.D. thesis, Cornell University, Ithaca, NY. 212.

Icenogle, R. D., and E. L. Elson. 1983. Fluorescence correlation spectroscopy and photobleaching recovery of multiple binding reactions. I. Theory and FCS measurements. *Biopolymers.* 22:1919–1948.

Janin, J. 1997. The kinetics of protein–protein recognition. *Proteins.* 28: 153–161.

Janin, J. 2000. Kinetics and thermodynamics of protein–protein interactions. *In* Protein–Protein Recognition. C. Kleanthous, Oxford University Press, New York. 1–32.

Kask, P., R. Gunther, and P. Axhausen. 1997. Statistical accuracy in fluorescence fluctuation experiments. *Eur. Biophys. J.* 25:163–169.

Kettling, U., A. Koltermann, P. Schwille, and M. Eigen. 1998. Real-time enzyme kinetics monitored by dual-color fluorescence cross-correlation spectroscopy. *Proc. Natl. Acad. Sci. U.S.A.* 95:1416– 1420.

Koppel, D. E. 1974. Statistical accuracy in fluorescence correlation spectroscopy. *Phys. Rev. A. Gen. Phys. (U.S.A.)* 10:1938–1945.

Koren, R., and G. G. Hammes. 1976. A kinetic study of protein–protein interactions. *Biochemistry.* 15:1165–1171.

Lamb, D. C., A. Schenk, C. Röcker, C. Scalfi-Happ, and G. U. Nienhaus. 2000. Sensitivity enhancement in fluorescence correlation spectroscopy of multiple species using time-gated detection. *Biophys. J.* 79: 1129–1138.

Langowski, J., and M. Tewes. 2000. Determination of DNA-ligand interactions by fluorescence correlation spectroscopy. *In* DNA–Protein Interactions: A Practical Approach. A. Travers and M. Buckle, editors. Oxford University Press, Oxford. 95–111.

Magde, D., E. Elson, and W. W. Webb. 1972. Thermodynamic fluctuations in a reacting system: measurement by fluorescence correlation spectroscopy. *Phys. Rev. Lett.* 29:705–708.

Magde, D., E. L. Elson, and W. W. Webb. 1974. Fluorescence correlation spectroscopy. II. An experimental realization. *Biopolymers.* 13:29–61.

Maiti, S., U. Haupts, and W. W. Webb. 1997. Fluorescence correlation spectroscopy: diagnostics for sparse molecules. *Proc. Natl. Acad. Sci. U.S.A.* 94:11753–11757.

Mertz, J. 1998. Molecular photodynamics involved in multi-photon excitation fluorescence microscopy. *Eur. Phys. J. D.* 3:53–66.

Meseth, U. 1996. Structural and functional investigations of channel forming peptides in lipid membranes. Ph.D. thesis, Ecole Polytechnique Fédéral de Lausanne, Lausanne, Switzerland. 95–140. *http://icpsg3.epfl.ch/Lit/PhDtheses/thesisMeseth/*

Meseth, U., T. Wohland, R. Rigler, and H. Vogel. 1999. Resolution of fluorescence correlation measurements. *Biophys. J.* 76:1619–1631.

Meyer-Almes, F. J., K. Wyzgol, and M. J. Powell. 1998. Mechanism of the α-complementation reaction of *E. coli* β-galactosidase deduced from fluorescence correlation spectroscopy measurements. *Biophys. Chem.* 75:151–160.

Müller, J. D., Y. Chen, and E. Gratton. 2000. Resolving heterogeneity on the single molecular level with the photon-counting histogram. *Biophys. J.* 78:474–486.

Northrup, S. H., and H. P. Erickson. 1992. Kinetics of protein–protein association explained by Brownian dynamics computer simulation. *Proc. Natl. Acad. Sci. U.S.A.* 89:3338–3342.

Pack, C. G., G. Nishimura, M. Tamura, K. Aoki, H. Taguchi, M. Yoshida, and M. Kinjo. 1999. Analysis of interaction between chaperonin GroEL and its substrate using fluorescence correlation spectroscopy. *Cytometry.* 36:247–253.

Pecht, I., D. Lancet. 1977. Kinetics of antibody–hapten interactions. *In* Chemical Relaxation in Molecular Biology. I. Pecht, and R. Rigler, editors. Springer-Verlag, Berlin. 306–338.

Qian, H. 1990. On the statistics of fluorescence correlation spectroscopy. *Biophys. Chem.* 38:49–57.

Rauer, B., E. Neumann, J. Widengren, and R. Rigler. 1996. Fluorescence correlation spectrometry of the interaction kinetics of tetramethylrhodamin α-bungarotoxin with *torpedo californica* acetylcholine receptor. *Biophys. Chem.* 58:3–12.

Rigler, R., J. Widengren, and Ü. Mets. 1992. Interactions and kinetics of single molecules as observed by fluorescence correlation spectroscopy. *In* Fluorescence Spectroscopy: New Methods and Applications. O.S. Wolfbeis, editor. Springer-Verlag, New York. 13–24.

Rigler, R., U. Mets, J. Widengren, and P. Kask. 1993. Fluorescence correlation spectroscopy with high count rate and low background: analysis of translational diffusion. *Eur. Biophys. J.* 22:169– 175.

Rippe, K. 2000. Simultaneous binding of two DNA duplexes to the NtrC-enhancer complex studied by two-color fluorescence cross-correlation spectroscopy. *Biochemistry.* 39:2131–2139.

Schatzel, K., M. Drewel, and S. Stimac. 1988. Photon correlation measurements at large lag times: improving statistical accuracy. *J. Mod. Opt.* 35:711–718.

Schreiber, G., and A. R. Fersht. 1996. Rapid, electrostatically assisted association of proteins. *Natl. Struct. Biol.* 3:427–431.

Schüler, J., J. Frank, U. Trier, M. Schäfer-Korting, and W. Saenger. 1999. Interaction kinetics of tetramethylrhodamine transferrin with human transferrin receptor studied by fluorescence correlation spectroscopy. *Biochemistry.* 38:8402–8408.

Schwille, P., J. Bieschke, and F. Oehlenschläger. 1997a. Kinetic investigations by fluorescence correlation spectroscopy: the analytical and diagnostic potential of diffusion studies. *Biophys. Chem.* 66:211–228.

Schwille, P., F. J. Meyer-Almes, and R. Rigler. 1997b. Dual-color fluorescence cross-correlation spectroscopy for multicomponent diffusional analysis in solution. *Biophys. J.* 72:1878–1886.

Schwille, P., U. Haupts, S. Maiti, and W. W. Webb. 1999. Molecular dynamics in living cells observed by fluorescence correlation spectroscopy with one- and two-photon excitation. *Biophys. J.* 77:2251–2265.

Thompson, N. L. 1991. Fluorescence correlation spectroscopy. *In* Topics in Fluorescence Spectroscopy: Techniques. J. R. Lakowicz, editor. Plenum Press, New York. 337–378.

Tjernberg, L. O., A. Pramanik, S. Björling, P. Thyberg, J. Thyberg, C. Nordstedt, K. D. Berndt, L. Terenius, and R. Rigler. 1999. Amyloid β-peptide polymerization studied using fluorescence correlation spectroscopy. *Chem. Biol.* 6:53–62.

Van Craenenbroeck, E., and Y. Engelborghs. 2000. Fluorescence correlation spectroscopy: molecular recognition at the single molecule level. *J. Mol. Recog.* 13:93–100.

Wei, J., and C. D. Prater. 1962. The structure and analysis of complex reaction systems. *Adv. Catalysis*. 13:203–392.

Weisstein, E. W. 1999. CRC Concise Encyclopedia of Mathematics. CRC Press LLC, New York.

Widengren, J., U. Mets, and R. Rigler. 1995. Fluorescence correlation spectroscopy of triplet states in solution—a theoretical and experimental study. *J. Phys. Chem.* 99:13368–13379.

Widengren, J., and R. Rigler. 1998. Fluorescence correlation spectroscopy as a tool to investigate chemical reactions in solutions and on cell surfaces. *Cell. Mol. Biol.* 44:857–879.

Widengren, J., E. Schweinberger, S. Berger, and C. A. M. Seidel. 2001. Two new concepts to measure fluorescence resonance energy transfer via fluorescence correlation spectroscopy: theory and experimental realizations. *J. Phys. Chem. A.* 105:6851–6866.

Wohland, T., K. Friedrich, R. Hovius, and H. Vogel. 1999. Study of ligand-receptor interactions by fluorescence correlation spectroscopy with different fluorophores: evidence that the homopentameric 5-hydroxytryptamine type 3As receptor binds only one ligand. *Biochemistry.* 38:8671–8681.

Wohland, T., R. Rigler, and H. Vogel. 2001. The standard deviation in fluorescence correlation spectroscopy. *Biophys. J.* 80:2987–2999.